



Why Is Height-Dependent Mixing Observed in Stratocumulus?

Zeen Zhu¹, Fan Yang¹, Steven Krueger², Yangang Liu¹

¹Environmental Science and Technologies Department, Brookhaven National Laboratory, Upton, NY, 11973, USA

²Department of Atmospheric Science, University of Utah, Salt Lake City, UT, 84112, USA

Correspondence to: Zeen Zhu (zzhu1@bnl.gov)

Abstract. Recent aircraft measurements in stratocumulus clouds suggest that entrainment mixing is inhomogeneous (IM) near cloud top and homogeneous (HM) within the cloud. However, this proposed height-dependence of mixing transition is uncertain because of artifacts involved in the aircraft measurements. In this study, we use the Explicit Mixing Parcel Model to simulate mixing scenarios in stratocumulus clouds and reconstruct the virtual aircraft measurements to investigate the mixing signature. Results show that, from the aircraft-measurement perspective, the mixing signature always exhibits IH characteristic near cloud top and HM characteristic within cloud, independent of the types of the local entrainment-mixing process. The appearance of the vertical IM-to-HM transition is essentially a collective behavior of multiple parcels sampled at the same height, experiencing distinct entrainment-mixing-evaporation histories. This bulk view of mixing process, which is widely used for aircraft measurements, could lead to misinterpretations of the true mixing mechanism occurring in clouds. Our result underscores the limitations of using aircraft measurements to identify the local entrainment-mixing mechanism at the process level.



33

34

35 **1. Introduction**

36 Entrainment-mixing is a critical cloud process and plays important roles in simulating precipitation
37 formation, radiative properties and macroscopic structures (Lasher-Trapp et al., 2005; Baker et al.,
38 1980; Lehmann et al., 2009; Magaritz-Ronen et al., 2014; Chosson et al., 2007). In the
39 stratocumulus, entrainment-mixing is initiated near cloud top where the dry, warm free-
40 troposphere air is partially mixed with the cloudy air and then entrained (Wood, 2012). After
41 entrainment, cloud droplets start to evaporate in a subsaturated environment along with the mixing
42 process. Depending on the efficiency of mixing and evaporation, two mixing scenarios are
43 generally considered: homogeneous mixing (HM) and inhomogeneous mixing (IM) (Latham and
44 Reed, 1977; Baker et al., 1980). For HM, turbulent mixing is much faster than droplet evaporation.
45 Under the extreme condition, the cloudy air is mixed immediately with the entrained air such that
46 all cloud droplets are exposed to the same sub-saturation environment, resulting in reduced droplet
47 size and unchanged number concentration. For the IM, turbulent mixing is slower than evaporation.
48 Under the IM condition, cloud droplets adjacent to the dry entrained air are quickly evaporated
49 while leaving the remaining droplets unaffected.

50 Over the recent decades, a consensus has emerged from aircraft observations across multiple field
51 campaigns that stratocumulus clouds tend to exhibit IM signature near the cloud top and a HM
52 signature in the mid-levels (Yum et al., 2015; Yeom et al., 2021; Desai et al., 2021; Wang et al.,
53 2009; Gao et al., 2021). One hypothesis to explain this behavior is the “vertical circulation”
54 concept which is proposed by Wang et al. (2009), further refined by Yum et al. (2015) and detailed
55 in Yeom et al. (2021). Specifically, after entrainment occurs near cloud top, the cloud parcel starts
56 to descend. The droplets in the diluted descending parcels evaporate and reduce the particle sizes.
57 Therefore, if the mid-level cloud is horizontally sampled by the aircraft, droplets are likely to be
58 evaporated in the diluted regions than those in the undiluted regions, leading to the HM signature
59 in the middle of cloud. Yeom et al. (2023) further conducted experiments in the cloud chamber by
60 injecting dry air into the well-mixed cloud to mimic the entrainment–mixing process. Result shows
61 that cloud microphysical responses to entrainment and mixing are locally inhomogeneous and
62 globally homogeneous, implying that the global versus local sampling of clouds can lead to
63 contradictory mixing results. These studies provide critical insights to reevaluate the applicability
64 of using aircraft measurements for HM/IM mixing classification.

65 Conventionally, cloud microphysical properties (e.g., droplet number and size) measured by
66 aircraft flying along a horizontal path are used to calculate the mixing metrics (see section 2.2) for
67 IM/HM classification. However, this aircraft-based perspective is known with several issues: 1):
68 the global mean cloud properties are not representative of the cloud structures at small scales. For
69 instance, Allwayin et al. (2024) utilizes holographic measurements showing that droplet size
70 distributions are more narrow at small scales than those at whole-cloud averages. 2) If the mixing
71 in each small sampling is inhomogeneous, then an average of several samplings may lead to



72 apparent homogeneous mixing (Burnet and Brenguier, 2007); 3) the aircraft flying along a path at
73 the same height measures a collection of mixed air parcels with different entrainment-mixing
74 stages, this collected behavior from various mixing parcels may not represent the original mixing
75 process in each individual parcel (Yeom et al., 2023). In this study, we revisit the applicability of
76 using aircraft measurements for mixing identification. We design a simulation framework based
77 on the Explicit Mixing Parcel Model (EMPM) to emulate the aircraft measurements in the Sc. We
78 show that, using aircraft measurements, the mixing behavior in Sc is always identified as IH near
79 cloud top and HM within clouds, regardless of the local mixing scenario within individual parcels.

80 The layout of this paper is organized as follows: Section 2 introduces the EMPM model, including
81 the adapted assumptions and the experiment set up. The mixing metrics used for HM/IM
82 identification applied in this study are introduced. In Section 3, the EMPM simulations are
83 analyzed from two perspectives: bulk and local. We show that, based on the same simulation
84 output, the mixing process in clouds may exhibit differently from the two perspectives; this
85 discrepancy is the key to understanding the limitations of aircraft measurements. In section 3, we
86 also conducted an additional isobaric mixing experiment to isolate the mixing and adiabatic
87 warming process which are coexisting in previous experiments. In Section 4, we explain the
88 phenomenon of the IM-HM transition in Sc and discuss the insights on future mixing studies.
89 Finally, a conclusion constitutes Section 5.

90

91 **2. Methods**

92 **2.1 Experiment Design**

93 The Explicit Mixing Parcel Model (EMPM) was developed by Krueger et al. (1997) to simulate
94 the evolution of cloud thermodynamic properties influenced by turbulent mixing in a rising cloudy
95 parcel. The EMPM can resolve fine-scale variability in the 1D domain down to the smallest
96 turbulent scales (about 1 mm) and calculate the growth/evaporation of individual cloud droplet
97 based on each droplet's local environment Su et al. (1998). One unique characteristic of the EMPM
98 is applying the linear eddy model (Kerstein, 1991) to simulate turbulent deformation and molecular
99 diffusion separately as an explicit representation of the turbulent mixing process. Specifically,
100 turbulent deformation is represented by a sequence of discrete rearrangement events along the 1D
101 domain, where the scalar field is randomly rearranged using a “triplet map” approach detailed in
102 (Krueger et al., 1997). Molecular diffusion is calculated with the 1D diffusion equation. With the
103 capabilities of resolving fine-scale variations and explicitly simulating turbulent mixing, the
104 EMPM is recognized as a unique and extensively used tool for entrainment and mixing studies (Lu
105 et al., 2013; Tölle and Krueger, 2014).

106 To emulate the aircraft measurements using the EMPM, three assumptions are made in this study:
107 1) entrainment occurs at cloud top; 2) after each entrainment event, the parcel undergoing mixing
108 descends from cloud top; 3) the virtual aircraft samples sufficient cloudy parcels along a path at
109 the same height, and those cloudy parcels experience various degrees of entrainment near the cloud
110 top. The first and second assumptions are satisfied for stratocumulus where the turbulent eddies



111 and evaporative cooling drives entrainment at cloud top (Wood, 2012). The third assumption is
112 proposed to mimic the aircraft measurements in real stratocumulus clouds.

113 The simulation design is illustrated in Fig. 1a. We consider a virtual aircraft that flies at a typical
114 speed of 100 m s^{-1} within the cloud, measuring droplet properties at 5 Hz along the leg. Over 2
115 second interval, the aircraft traverses 200 meters, consisting of 10 in-situ samples, each 20 meters
116 in length. In the EMPM, each in-situ sample is configured as a one-dimensional domain with a
117 length of 20 m and the width/depth of 1 mm, resulting in a total volume of 20 cm^3 (right panel of
118 Fig. 1a). The detailed model configuration is shown in Table. 1. The initial droplet number
119 concentration is set as 80 cm^{-3} , consisting of monodisperse haze particles of radius $0.216 \mu\text{m}$. The
120 simulation begins with adiabatic lifting of the parcel at a constant velocity of 1 m s^{-1} until it reaches
121 the cloud top. The parcel then encounters entrainment, during which subsaturated air replaces a
122 segment of the cloudy parcel of equal size. The fraction of subsaturated entrained air relative to
123 the domain size is referred as the entrainment fraction (EF). For instance, Fig. 1a illustrates an
124 entrainment event with EF of 0.5, meaning that 50% of the cloudy parcel, which is effectively 10
125 m, is replaced by the entrained subsaturated air. We assume that the entrained dry air is Cloud
126 Condensation Nuclei (CCN) free thus no CCN is entrained into clouds. After entrainment, the
127 parcel descends adiabatically at a velocity of -1 m s^{-1} . As the parcel descends, the cloudy air and
128 the entrained air undergo finite-rate mixing, during which droplets encounter the subsaturated air
129 and partially or completely evaporate. The number and size of droplets in the domain are updated
130 at each time step (1s) until all the droplets are completely evaporated.

131 For each experiment, a total of ten EMPM simulations is conducted with the same initial setting
132 but with various EFs from 0 to 0.9, representing multiple entrainment events occurring at the cloud
133 top. Combining all the simulation results produces the collective output illustrated in Fig. 1b. In
134 this study, we will analyze the output from two perspectives: “bulk” and “local”. The bulk-based
135 perspective emulates the aircraft measurements in clouds, where multiple parcels are sampled at
136 the same height with each one experiencing distinct entrainment-mixing histories. The local-based
137 perspective tracks the evolution of cloud microphysical properties in individual parcel after
138 entrainment, representing the “true” mixing process within the parcel.

139 To drive the simulations, the idealized thermodynamical profile (Fig. 2) is constructed from the
140 observations on June 30th, 2017 during the Aerosol and Cloud Experiments in the Eastern North
141 Atlantic (ACE-ENA) field campaign (Wang et al., 2022). It is noted that a strong inversion layer
142 exists at 970 m, defining the cloud top height in Table 1. For this study, three experiments (Control,
143 Dry, and Turbulent) are conducted to represent different entrainment-mixing scenarios. For the
144 Control simulation, the Eddy Dissipation Rate (EDR) is adapted from the observation as 0.0025
145 $\text{m}^2 \text{s}^{-3}$, representing a typical Sc environment. The thermodynamics of the entrained air is estimated
146 as the parcel at 10 m above cloud top experiencing adiabatic descent to cloud top. Particularly, the
147 entrained air temperature and water vapor is estimated as 285.77 K and $8.6 \times 10^{-3} \text{ g/kg}$. Besides the
148 control case, two sensitivity cases have been conducted: “Dry” and “Turbulent”. For the “Dry”
149 experiment, the model setup is the same as the control one except the entrained air property is
150 estimated using the parcel at 20m above cloud top experiencing adiabatic descent to cloud top,



151 where the air temperature and water vapor is estimated as 288 K and 7.8×10^{-3} g/kg. The selection
152 of the entrained parcel distance from cloud top is arbitrary and does not affect the conclusions of
153 this study. For the “Turbulent” experiment, the model setting is same as the Control one except
154 the EDR is set as $0.01 \text{ m}^2 \text{ s}^{-3}$, representing a more turbulent environment.

155

156 **2.2 Entrainment Mixing Metrics**

157 With the aircraft measurements, the mixing process is characterized by overlaying the cloud
158 properties on the mixing diagram and analyzing their collective behaviors (Burnet and Brenguier,
159 2007; Lehmann et al., 2009; Yum et al., 2015). In this study, the simulation result is displayed in
160 mixing diagrams similar to those used in the aircraft-measurement studies. In addition, we adapt
161 the homogeneous mixing degree (ψ) to identify the mixing process from the local-based
162 perspective. The mixing diagram and the associated metrics are introduced in the following.

163 **2.2.1 n - r^3 Mixing Diagram**

164 The n - r^3 mixing diagram is commonly applied to characterize the mixing process in clouds. In the
165 diagram, the horizontal and vertical axes represent the normalized number concentration (n) and
166 the average of the third moment of droplet radius (r^3). The measurements are normalized by their
167 theoretical values assuming the cloud parcel ascends adiabatically. For extreme IM, droplet
168 number is further reduced while the size remains constant, therefore the measurements are
169 horizontally aligned. For extreme HM, droplet number remains unchanged after dilution, while the
170 size is reduced due to evaporation. In reality, the mixing can be between the two extreme mixing
171 types, and thus both droplet number and size may be reduced in the diagram.

172 **2.2.3 $LWC - \tau_{\text{phase}}$ mixing diagram**

173 The L - τ_{phase} mixing diagram was proposed by Yeom et al. (2021) with x -coordinates as the
174 logarithm of liquid water content (L) and y -coordinates as the logarithm of phase relaxation time
175 (τ_{phase}). L is calculated as:

$$176 \quad L = \frac{4\pi\rho_L n r^3}{3}$$

177 where n and r represent the number concentration and droplet radius, and ρ_L is the density of
178 liquid water.

179

180 The phase relaxation time (τ_{phase}) characterizes how rapidly an equilibrium vapor saturation is
181 reached by evaporation of a population of droplets (Lehmann et al., 2009; Jeffery and Reisner,
182 2006). For the EMPM simulation output, τ_{phase} is calculated following the method applied in
183 Tölle and Krueger (2014):

$$184 \quad \tau_{\text{phase}} = \frac{1}{4\pi D_v N} \frac{R_v + a}{R_v^2}$$



185 where N and R_v represent the domain-mean droplet number and radius estimated at the time
186 immediately following the entrainment event. D_v is the molecular diffusivity of water vapor and
187 is taken as $0.256 \text{ cm}^2\text{s}^{-1}$. a is the accommodation length taken as $2 \mu\text{m}$.

188

189 To interpret the L - τ_{phase} mixing diagram, linear regression is performed between the logarithm
190 of L and τ_{phase} dataset and the corresponding slope is used for mixing classification: the slope of
191 -1 represents extreme IM, while the HM should asymptote to the line with slope of $-1/3$.

192

193 2.2.3 Homogeneous mixing degree

194 Based on the n - r^3 mixing diagram, Lu et al. (2013) proposed the homogeneous mixing degree
195 following the calculation:

$$196 \quad \beta = \tan^{-1} \left(\frac{\frac{r_v^3}{r_{av}^3} - 1}{\frac{n}{n_a} - \frac{n_h}{n_a}} \right)$$

197 where r_v and r_{av} represent the volume-mean radius and the adiabatic radius of droplets, n is the
198 number concentration, n_a is the adiabatic number concentration, n_h is the number concentration
199 immediately following the entrainment event but prior to evaporation and accounts for the dilution
200 by entrainment; The parameter β effectively calculates the angle, with unit of radian, from the
201 extremely IM line (detailed illustration is shown in Fig. 1 in Lu et al. (2013)).

202 β is commonly normalized by $\pi/2$ to represent the homogeneous mixing degree (ψ):

$$203 \quad \psi = \frac{\beta}{\pi/2}$$

204 ψ ranges from 0 to 1, with large values indicating IM and small ψ indicating HM. Since ψ is
205 estimated upon each parcel instead of a collective datapoints, we apply ψ to characterize the local
206 mixing process within the parcel.

207

208

209

210 3. Results

211 3.1 Cloud Properties from the EMPM simulation

212 The simulated domain-averaged cloud properties under various entrainment events are shown in
213 Fig. 3. When the parcel ascends adiabatically, the LWC linearly increases from cloud base (i.e.
214 745 m) to cloud top with the maximum value of 0.42 g m^{-3} (red line in Fig. 3a). The domain-
215 averaged cloud droplet radius increased to $10.7 \mu\text{m}$ (red line in Fig. 3b). Correspondingly, a total



of 1600 droplets is activated at cloud base and the number remain unchanged towards cloud top. Considering the EMPPM domain of 20 cm^3 , the number concentration within the undiluted ascending parcel is 80 cm^{-3} . As introduced in Sec 2.1, the parcel descent immediately after reaching cloud top. When no entrainment occurs at the cloud top, the simulated cloud properties within the descending parcel is shown as the blue line in Fig. 3. It is noticed that LWC and the droplet radius do not follow the trajectory of the ascending parcel but with slightly enhanced value. This enhanced radius/LWC is caused by the hysteresis effect manifested as the time-lag adjustment of the parcel supersaturation responding to the change of dynamics (Yang et al., 2018). Specifically, as the parcel starts moving downward as a consequence of the changed velocity from 1 ms^{-1} to -1 ms^{-1} , the supersaturation within the parcel remains positive with value of 0.47 % (red line in Fig. 3d). Consequently, the droplet continues to grow until the supersaturation is removed. It is shown that the supersaturation turns to negative at the height of 943m, which is 7 m down from cloud top. The extra growth over this 7m distance led to a larger LWC and radius in the downward branch (Fig. 3a, c).

For the descending parcels with various entrainment events, LWC and droplet number reduce instantaneously at cloud top (Fig. 3a, c) due to the replacement by entrained air. Meanwhile, the domain-mean radius remains constant at cloud top (Fig.3 b) as the evaporation-mixing process has not yet begun. As the parcel descends, LWC, droplet radius and number decrease due to evaporation. The extent of the reduction depends on the entrainment fraction. For strong entrainment event, the mixed parcel is much drier thus experiencing stronger evaporation, leading to lower LWC, smaller radius, and fewer droplets. Under large EF, droplets within the parcel are completely evaporated at a higher altitude. For instance, for the EF of 0.4 (black line in Fig. 3), droplets are evaporated at 862 m, which is 88 m below the cloud top (Fig. 3c).

239

240 **3.2 Entrainment Mixing Behavior within Clouds**

241 **3.2.1 Bulk Perspective**

We use the two mixing diagrams to analyze the EMPPM simulations from the aircraft-based perspective. In the $n-r^3$ mixing-diagram (Fig. 4a, c, e), droplet number and r^3 are normalized by the value in the descending parcel without entrainment occurring (blue line in Fig. 3b, c). For the control experiment (Fig. 4a), the collective behavior of the 10 simulations with different EFs shows reduced droplet number but unchanged radius at 5m below cloud top (circles in Fig. 4a). The reduced number is caused by the entrainment when a given fraction of the domain is instantaneously replaced by the droplet-free air. At 5m below cloud top, droplets have not yet experienced strong evaporation because only 5 s has elapsed since the entrainment event. To better visualize the mixing signature at different heights, polynomial lines are fitted based on the normalized $n-r^3$ diagram. The fitted line at 5 m below cloud top is horizontally aligned reasonably well with the normalized $r^3 = 1$ (black line in Fig. 4a), exhibiting a typical IM signature. This IM phenomenon is echoed in the $L-\tau_{\text{phase}}$ mixing diagram: the slope of the linear regression of the datasets at 5 m below cloud top is -0.81 (circles in Fig. 4b), which is close to the IM reference line with the slope of -1.



256 As the parcels descend deeper into the cloud, those with different EFs exhibit distinct evaporation
257 histories, leading to contrasting mixing signatures. Taking the control experiment at 50 m below
258 cloud top (squares in Fig. 4a) as an example, the normalized r^3 is reduced to 0.48 for the parcel
259 with EF equals 0.8, while the normalized r^3 is 0.92 for the parcel with EF equals 0.1. As a result,
260 the collected behavior of all the parcels at this level exhibit HM signatures (red line in Fig. 4a)
261 with reduced droplet numbers and radii. It is further noted that the HM signature is more prominent
262 deeper into the cloud (i.e., further away from the cloud top). Comparing the fitted lines from two
263 height levels (red and blue lines in Fig. 4a), parcels at 200 m below cloud top show greater
264 reduction of radius compared to the parcels at 50 m below cloud top. This transition of the mixing
265 signatures is more evident in the L - τ_{phase} mixing diagram (Fig. 4b). As the distance from the cloud
266 top increases, the collective datapoints rotate counterclockwise from the IM (red line) to the HM
267 (blue line) reference line. Specifically, for heights at 5m (circles), 50m (squares) and 200m
268 (triangles) from cloud top, the slopes of the linear regression are -0.81, -0.32 and -0.28, exhibiting
269 a stronger HM degree deeper into cloud.

270 The two sensitivity experiments (i.e., Dry and Turbulent) lead to similar conclusions as the Control
271 one with slightly different behavior. When the entrained air is drier, the mixed parcel experiences
272 stronger evaporation thus exhibiting a small degree of HM signature near cloud top. In the Dry
273 experiment (Fig. 4b), the normalized r^3 at 5 m below cloud top decreases by 17% in the simulation
274 with an EF of 0.9, causing the fitted line to bend downward toward smaller radii in the large EF
275 regime (black line in Fig. 4b). However, it is still clear that near cloud top the mixing is
276 predominantly IM with a significant reduction of droplet number and a small reduction of radius.
277 This IM-dominated signature is also identified in the L - τ_{phase} mixing diagram (Fig. 4d) in which
278 parcels near cloud top (circles) align well with the IM reference line (red dashed line). In the
279 Turbulent experiment (Fig. 4e, f), the mixing signature is similar to the Control one near cloud top
280 but shows differences deeper into the cloud. For a given normalized n , the Turbulent experiment
281 is characterized by a greater reduction of radius compared to the Control one. For instance, at 200
282 m from cloud top, where the normalized n equals 0.6, the normalized r^3 for the Control and
283 Turbulent experiments are 0.7 and 0.48, respectively. This large reduction of droplet size is
284 expected as strong turbulence favors efficient mixing and enhance the HM signature.

285 Overall, despite the different thermodynamics and dynamics of the entrained air, simulations show
286 a clear IM feature near cloud top and HM within the cloud, with greater degree of HM deep into
287 the cloud. These model-based results are consistent with the aircraft measurements in Sc (Yum et
288 al., 2015; Yeom et al., 2021), thus providing a strong foundation for more detailed investigations
289 in the next section.

290
291
292
293
294
295
296



297 3.2.2 Local Perspective

298 In this section the EMPM simulations in Sec 3.2.1 are interpreted from the local-based perspective
 299 as introduced in Fig. 1. Specifically, instead of analyzing parcels with different EFs at given height,
 300 we evaluate the mixing process of each parcel by tracking its history. Figure 5a shows the $n-r^3$
 301 mixing diagram for four parcels with EF of 0.1, 0.3, 0.5, and 0.7. The parcels initially follow a
 302 near-vertical path (i.e., indicating a reduction in droplet size with minimal change in number
 303 concentration) near the cloud top, then gradually tilt toward the smaller number regime. These
 304 features show HM near cloud top and the mixing more tends to inhomogeneous deeper into cloud.
 305 The strongest HM signature is observed for the parcel with EF = 0.1 (blue symbols), where at 50
 306 m below the cloud top, the normalized r^3 decreases by 18%, while the normalized number
 307 decreases by only 1.5%. This behavior highlights the dominance of HM near cloud top.

308 To quantitatively describe the mixing process in each parcel, we adapt the homogeneous mixing
 309 degree ψ proposed by Lu et al. (2013). As introduced in Sec 2.2, ψ is evaluated based on the $n-r^3$
 310 mixing diagram by calculating the relative changes of droplet size and number after each mixing
 311 event. Since estimating ψ only requires the change of cloud microphysics within each parcel, it is
 312 suitable to illustrate the mixing process from the local perspective. For the four selected parcels,
 313 ψ consistently decreases from cloud top to base (Fig. 5b). As $\psi = 1$ indicates extremely HM, the
 314 large ψ at Fig. 5b indicates strong HM at cloud top. Deeper into the cloud, ψ decreases, indicating
 315 a weakening of HM and an increasing influence of IM. This behavior holds true for all the four
 316 simulations regardless of the entrainment degree. Parcel with EF 0.1 has the largest ψ throughout
 317 the cloud and exhibits the most pronounced HM signature. Parcel with EF of 0.3 and 0.5 have ψ
 318 decreasing from 1 to 0.65 and 0.76 at 100 below cloud base.

319 The HM–IM transition observed from the local perspective appears to contradict the mixing
 320 behavior suggested by the bulk perspective. We propose that this inconsistency arises from the
 321 differing analytical perspectives. The local perspective indicated in Fig. 5 follows the continuous
 322 evolution of individual parcel, revealing the “true” mixing processes. While the bulk perspective
 323 captures a “snapshot” of an ensemble of parcels, each with distinct entrainment and mixing
 324 histories. Near the cloud top, the entrained air replaces the cloudy air and instantaneously reduce
 325 the droplet number. Immediately following entrainment, parcels with large EF experience larger
 326 reductions of droplet number, while evaporation has not yet efficient enough to reduce droplet size.
 327 Thus, a collection of multiple parcels with different entrainment events generates an IM signature.
 328 As the parcel descends deeper into the cloud, mixing with dry air continues and evaporation
 329 becomes efficient, leading to a reduction in droplet size. Parcels with larger EF experiencing
 330 stronger evaporation and results in more pronounced decrease in droplet size and number.
 331 Consequently, a collection of parcels with different EF tends to exhibit a HM signature deeper into
 332 the cloud.

333 Based on this reasoning, we further propose that from the bulk perspective, mixing is always
 334 manifested as IM near cloud top and HM towards cloud base, regardless of the mixing process
 335 exhibited from local perspective. To testify this hypothesis, we conduct a strict IM experiment
 336 with the same configuration as the Control experiment but setting an extremely low EDR value of
 337 $10^{-14} \text{ m}^2 \text{ s}^{-3}$. This nonrealistic EDR value results in low mixing efficiency in the EMPM simulation



where 100 steps of diffusion (e.g. evaporation) are performed per turbulent mixing step. As a comparison, for the “Turbulent” experiment where EDR is $0.01 \text{ m}^2 \text{ s}^{-3}$, the EMPM performs 100 mixing steps per diffusion step. Thus, the conducted IM experiment ensures strict IM scenario with evaporation much faster than the turbulent mixing.

The mixing process of the strict IM experiment from the local perspective is shown in Fig. 6. In the $n-r^3$ mixing diagram, the parcel experiencing greater reduction of number compared with radius. Take the simulation with EF of 0.1 (blue symbol in Fig. 6a) for example, from 2m to 150m from cloud top, droplet number is reduced by 6% while the normalized r^3 is only reduced by 0.8%. The evolution of ψ within clouds (Fig. 6b) indicate an IM-HM transition from cloud top to base. Specifically, ψ increase from 0 to approximately 0.4 through the clouds, suggesting strong IM feature near cloud top and an increase degree of HM at lower levels. The negative β near cloud top is caused by the growth of droplet after entrainment, which may be caused by the remaining supersaturated environment at cloud top as discussed in Fig. 3d.

Although strong IM signature is identified for each parcel, the collective behavior of multiple parcels still exhibits IM near cloud top and HM within cloud. At 2m below cloud top, parcels with various EFs are aligned horizontally (circles in Fig. 6a) and is manifested as IM signature. At 150 m below the cloud top, stronger entrainment events lead to greater reductions in droplet radius. For the parcel with EF = 0.7 (yellow symbols), the normalized r^3 decreases by 13%, whereas for the parcel with EF = 0.1, the reduction is only 0.8%. As a result, connecting the parcels at 150m below cloud top (inverted triangles in Fig. 6a) reveals HM signature. It is noticeable that the reduction of droplet size in Fig. 6a is significantly smaller than the control experiment as shown in Fig. 5a. This difference is expected as the turbulent mixing is strongly inhibited in Fig. 6a, thus the entrained dry air cannot efficiently mix with cloudy air, which eventually inhibits evaporation of droplets. Nevertheless, the experiments shown in Fig. 5 and Fig. 6 demonstrate that, from the bulk perspective, mixing behavior consistently exhibits IM near the cloud top, with an increasing signature of HM deeper within the cloud, regardless of the local mixing processes occurring in individual parcels.

3.3 Isobaric-Mixing Experiment

In previous sections, we have reconstructed the mixing behavior in Sc using EMPM simulations which is consistent with the aircraft-based measurements. However, the non-isobaric mixing process in previous experiments may lead to ambiguity for mixing interpretation. Specifically, when droplets evaporate in a descending parcel, the subsaturated environment can be caused by adiabatic warming and non-isobaric mixing. To isolate these two effects, we conduct an isobaric mixing experiment. The experiment setup is the same as the control one except after entrainment event near cloud top, the parcel velocity is set to 0 m s^{-1} . This setting ensures the parcel only experiencing isobaric mixing after the entrainment at cloud top.



Fig. 7 shows the mixing diagrams at three elapsed times after the entrainment event. At 3s, parcels with different EFs are closely aligned with the line of normalized $r^3 = 1$. Correspondingly, the slope of the fitted line in the L - τ_{phase} diagram is -0.81 (Circle in Fig. 7b). These two features suggest IM at the beginning of mixing process. At 15s, HM signature is identified with parcels of large EF experiencing greater reduction of radii and number (red line in Fig. 7a). At 90s, stronger reduction of droplets size and number indicating a more prominent HM signature (blue line in Fig. 7a). The L - τ_{phase} diagram echoes the stronger HM feature as mixing continuing with the fitted slope increases from -0.56 to -0.42 from 15s to 90s.

To better illustrate the mixing process as a function of time, the normalized standard deviation of water vapor is plotted for four experiments (Fig. 8a). Specifically, the standard deviation of water vapor (δ_{qv}) is calculated at each time step within the 1D domain with a domain size of 20 m and grid size of 1 mm. Then normalization is performed by dividing $\delta_{qv}(t)$ by δ_{qv} at 1 s after entrainment. The evolution of the variances of δ_{qv} can illustrate the mixing time scale (Tölle and Krueger, 2014). In Fig. 8a, δ_{qv} is maximum after the entrainment. As time goes by, q_v decreases as mixing occurs between the entrained air and cloudy air. Parcels with the small EF experience a short mixing time compared with those with large EF. For instance, the parcel with EF 0.3 needs 60 s to reach the equilibrium state (green line in Fig. 8a) while the one with EF 0.1 needs only 20 s (blue line in Fig. 8a) to homogenize water vapor within the domain.

The parcel-based mixing behavior for four parcels is shown in Fig. 8b. Tracking individual parcels, it is clearly shown that the parcel experiencing HM has a greater reduction of radii compared to number. The most extreme case is for the parcel with EF of 0.1 (blue symbols in Fig. 8b): during the mixing process the normalized r^3 decreases by 17% while the normalized number barely changes. Correspondingly, the ψ parameter decreases from 1 to 0.97 from 0 to 12 s, indicating extreme HM. Parcels with large EF exhibit HM signatures after a greater duration of mixing. For instance, ψ for the parcels with EF of 0.3 and 0.4 decrease from 1 to 0.7 at 80 s after entrainment, suggesting the HM signature is enhanced as the mixing proceeds.

In a nutshell, the isobaric mixing experiment exhibits similar results as shown in the previous experiments. The collective mixing behavior of multiple parcels exhibits IM at the beginning of mixing and HM at later time. The elapsed time in the isobaric mixing experiment is equivalent to the distance from cloud top for the non-isobaric mixing experiments. The true mixing process as indicated from the local-based perspective, on the other hand, may be completely different from the collective mixing behavior. This isobaric mixing experiment reinforces the conclusion that the IM-HM transition from the bulk perspective results from the sampling strategy in clouds rather than true mixing process in the parcel.



415 **4. Discussion**

416 Using multiple EMPM simulations, we successfully reproduce the commonly aircraft-observed
 417 result with IM near cloud top and HM within cloud. We further explain this phenomenon in Fig.
 418 9. The aircraft measurements include multiple cloud parcels experiencing different entrainment-
 419 mixing histories. In Sc, entrainment occurs at the cloud top where a horizontal fraction of cloudy
 420 air is replaced by the free atmosphere. If the entrained air is cloud droplet-free, the entrainment
 421 event instantaneously reduces droplet number. Parcels experiencing strong entrainment have
 422 greater reductions of droplet number. The moment after entrainment, the dry air has not yet mixed
 423 with cloudy air, which is required to generate strong evaporation, thus the domain-averaged size
 424 remains constant. A collection of multiple parcels at cloud top are aligned along a horizontal line
 425 indicating the IM signature. As the parcel descends into cloud, mixing and evaporation occur
 426 collectively to reduce droplet size and number. Parcels with strong entrainment at the cloud top
 427 are associated with large entrainment fraction, resulting in a drier environment compared to parcels
 428 with smaller EF. Deeper into the cloud, parcels with large EF experience stronger evaporation,
 429 leading to a greater reduction in both droplet size and number. The collective view of parcels with
 430 different EFs in the $n-r^3$ mixing diagram exhibits HM signature.

431

432 This explanation is essentially consistent with the “vertical circulation” hypothesis proposed by
 433 Yum et al. (2015). In this study we use the EMPM simulations for a thoughtful demonstration and
 434 aim to raise the awareness of this modeling approach for investigating entrainment-mixing
 435 processes. Particularly, the aircraft measurements should be interpreted with caution especially
 436 when multiple samples along the aircraft traverse are overlapped in the mixing diagram. The
 437 collective behavior of different samples at given altitude may exhibit a result which does not
 438 represent the true mixing mechanism of each sample. For the similar reason, the Large Eddy
 439 Simulation (LES) output should also be analyzed with caution. Collecting cloud properties along
 440 multiple grids at a given height in the model generates pseudo “aircraft-based measurements”,
 441 which may also lead to misinterpretation of the mixing process. Lagrangian-based models, with
 442 the capability of tracking the history of each parcel, should serve as a more suitable tool for mixing
 443 investigations (Hoffmann and Feingold, 2019; Lim and Hoffmann, 2024). From the observational
 444 perspective, while the Lagrangian-based tracking approach is not applicable, alternative
 445 measurement methods developed in recent decades is helpful to mitigate the mixing artifacts
 446 generated from the aircraft measurements. For instance, the Cloudkite platform deployed at the
 447 kite-stabilized balloons (Schröder, 2023) and the holographic imaging technique (Beals et al., 2015)
 448 can provide high spatio-temporally resolved measurements down to cm-scales. Such fine-
 449 resolution observations capture the local cloud mixing state more representatively, offering deeper
 450 insights into the entrainment mixing processes within clouds.

451

452

453

454



5. Conclusion

In this study, we conduct EMPM simulations to understand the entrainment-mixing process observed from aircraft measurements in stratocumulus cloud. Three experiments are conducted with different thermodynamic and turbulence environments. Each experiment consists of ten simulations, with each simulation representing a 20-meter parcel undergoing various entrainment degree at cloud top and distinct mixing history. The overall entrainment-mixing process for the simulations is analyzed from two views: the bulk-based and local perspective. The bulk perspective resembles the aircraft measurements in clouds and is illustrated by two commonly used mixing diagrams. The local perspective reflects the true mixing behavior in each parcel and is quantified by the homogeneous mixing degree (ψ) developed by Lu et al. (2013).

From the bulk perspective, the simulated mixing is identified as IM near cloud top and HM within cloud, which is consistent with the aircraft measurements in real clouds. However, this vertical progression primarily arises from the collective view of multiple parcels experiencing different mixing stages, in which strong evaporation in some parcels juxtapose with weak evaporation in others. This bulk view obscures the parcel's actual mixing process and leads to the appearance of a systematic IM-HM transition within cloud, even in cases where the underlying local mixing within each parcel could be substantially different. It is suggested that future mixing investigations in clouds should carefully re-examine the aircraft-based interpretation and consider incorporating Lagrangian approaches.

It is noted that the purpose of this study is to urge caution when interpreting aircraft measurements and LES simulations in entrainment-mixing research. This study does not aim to conclude the entrainment mixing behaviors in clouds. To advance the understanding of mixing processes in real clouds, emerging measurement technologies, such as the holographic detectors and tethered platforms, offer critical insights to observe mixing at the parcel scale. Additionally, for illustrative purposes, this study employs an idealized mixing framework in which each parcel evolves independently, with no mixing between parcels with differing entrainment histories. While a more sophisticated mixing scheme could better approximate observational realities, such complexity falls outside the scope of the present work.



491

492 **Code/Data availability:**

493 The EMPM codes used in this study is available upon request from the authors.

494

495 **Financial Support:**

496 Z. Zhu, F. Yang, Y. Liu were funded by the Department of Energy (DOE) as part of the
497 Atmospheric System Research (ASR) program under Contract DE-SC0012704. S. Krueger was
498 supported by NSF grant AGS-2133229.

499

500 **Author contribution:**

501 ZZ designed the methodology and carried out the analysis. FY contributed to the study design. SK
502 provided guidance on the use of the EMPM. YL assisted with the interpretation of results. ZZ
503 drafted the manuscript, with all co-authors contributing to revisions and editing.

504

505

506 **Competing interests:**

507 The corresponding author has declared that neither they nor their co-authors have any competing
508 interests.

509

510

511

512

513

514

515

516

517

518



519

520 **Reference**

- 521 Allwayin, N., Larsen, M. L., Glienke, S., and Shaw, R. A.: Locally narrow droplet size
522 distributions are ubiquitous in stratocumulus clouds, *Science*, 384, 528-532, 2024.
- 523 Baker, M., Corbin, R., and Latham, J.: The influence of entrainment on the evolution of cloud
524 droplet spectra: I. A model of inhomogeneous mixing, *Quarterly Journal of the Royal*
525 *Meteorological Society*, 106, 581-598, 1980.
- 526 Beals, M. A., Fugal, J. P., Shaw, R. A., Lu, J., Spuler, S. M., and Stith, J. L.: Holographic
527 measurements of inhomogeneous cloud mixing at the centimeter scale, *Science*, 350, 87-90,
528 2015.
- 529 Burnet, F. and Brenguier, J.-L.: Observational study of the entrainment-mixing process in warm
530 convective clouds, *Journal of the atmospheric sciences*, 64, 1995-2011, 2007.
- 531 Chosson, F., Brenguier, J.-L., and Schüller, L.: Entrainment-mixing and radiative transfer
532 simulation in boundary layer clouds, *Journal of the atmospheric sciences*, 64, 2670-2682, 2007.
- 533 Desai, N., Liu, Y., Glienke, S., Shaw, R. A., Lu, C., Wang, J., and Gao, S.: Vertical variation of
534 turbulent entrainment mixing processes in marine stratocumulus clouds using high-resolution
535 digital holography, *Journal of Geophysical Research: Atmospheres*, 126, e2020JD033527, 2021.
- 536 Gao, S., Lu, C., Liu, Y., Yum, S. S., Zhu, J., Zhu, L., Desai, N., Ma, Y., and Wu, S.:
537 Comprehensive quantification of height dependence of entrainment mixing between stratiform
538 cloud top and environment, *Atmospheric Chemistry and Physics*, 21, 11225-11241, 2021.
- 539 Hoffmann, F. and Feingold, G.: Entrainment and mixing in stratocumulus: Effects of a new
540 explicit subgrid-scale scheme for large-eddy simulations with particle-based microphysics,
541 *Journal of the Atmospheric Sciences*, 76, 1955-1973, 2019.
- 542 Jeffery, C. A. and Reisner, J. M.: A study of cloud mixing and evolution using PDF methods.
543 Part I: Cloud front propagation and evaporation, *Journal of the atmospheric sciences*, 63, 2848-
544 2864, 2006.
- 545 Kerstein, A. R.: Linear-eddy modelling of turbulent transport. Part 6. Microstructure of diffusive
546 scalar mixing fields, *Journal of Fluid Mechanics*, 231, 361-394, 1991.
- 547 Krueger, S. K., Su, C.-W., and McMurtry, P. A.: Modeling entrainment and finescale mixing in
548 cumulus clouds, *Journal of the atmospheric sciences*, 54, 2697-2712, 1997.
- 549 Lasher-trapp, S. G., Cooper, W. A., and Blyth, A. M.: Broadening of droplet size distributions
550 from entrainment and mixing in a cumulus cloud, *Quarterly Journal of the Royal Meteorological*
551 *Society: A journal of the atmospheric sciences, applied meteorology and physical oceanography*,
552 131, 195-220, 2005.
- 553 Latham, J. and Reed, R.: Laboratory studies of the effects of mixing on the evolution of cloud
554 droplet spectra, *Quarterly Journal of the Royal Meteorological Society*, 103, 297-306, 1977.
- 555 Lehmann, K., Siebert, H., and Shaw, R. A.: Homogeneous and inhomogeneous mixing in
556 cumulus clouds: Dependence on local turbulence structure, *Journal of the Atmospheric Sciences*,
557 66, 3641-3659, 2009.
- 558 Lim, J. S. and Hoffmann, F.: Life cycle evolution of mixing in shallow cumulus clouds, *Journal*
559 *of Geophysical Research: Atmospheres*, 129, e2023JD040393, 2024.
- 560 Lu, C., Liu, Y., Niu, S., Krueger, S., and Wagner, T.: Exploring parameterization for turbulent
561 entrainment-mixing processes in clouds, *Journal of Geophysical Research: Atmospheres*, 118,
562 185-194, 2013.

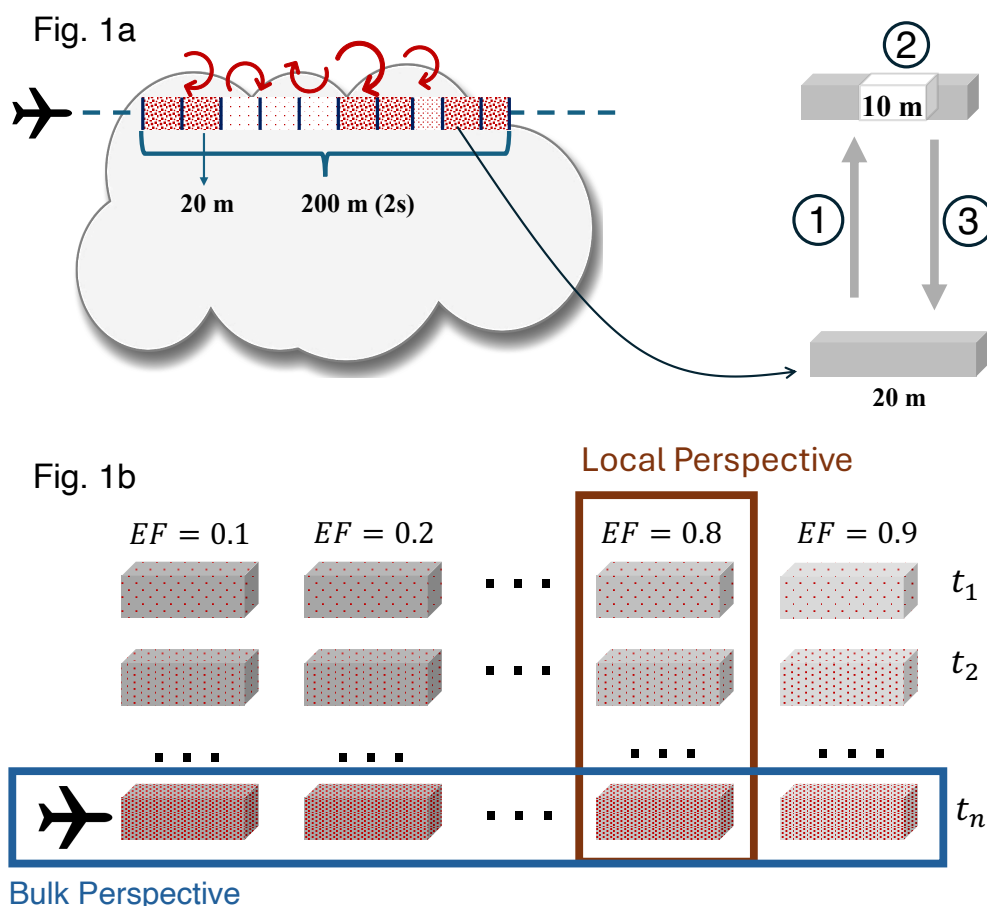


563 Magaritz-Ronen, L., Pinsky, M., and Khain, A.: Effects of turbulent mixing on the structure and
564 macroscopic properties of stratocumulus clouds demonstrated by a Lagrangian trajectory model,
565 *Journal of the Atmospheric Sciences*, 71, 1843-1862, 2014.
566 Schröder, M.: Cloud Microphysics Investigations with the Cloudkite Laboratory, Georg-August-
567 Universität Göttingen Göttingen, 2023.
568 Su, C.-W., Krueger, S. K., McMurtry, P. A., and Austin, P. H.: Linear eddy modeling of droplet
569 spectral evolution during entrainment and mixing in cumulus clouds, *Atmospheric research*, 47,
570 41-58, 1998.
571 Tölle, M. H. and Krueger, S. K.: Effects of entrainment and mixing on droplet size distributions
572 in warm cumulus clouds, *Journal of Advances in Modeling Earth Systems*, 6, 281-299, 2014.
573 Wang, J., Daum, P. H., Yum, S. S., Liu, Y., Senum, G. I., Lu, M. L., Seinfeld, J. H., and Jonsson,
574 H.: Observations of marine stratocumulus microphysics and implications for processes
575 controlling droplet spectra: Results from the Marine Stratus/Stratocumulus Experiment, *Journal*
576 *of Geophysical Research: Atmospheres*, 114, 2009.
577 Wang, J., Wood, R., Jensen, M. P., Chiu, J. C., Liu, Y., Lamer, K., Desai, N., Giangrande, S. E.,
578 Knopf, D. A., and Kollias, P.: Aerosol and cloud experiments in the Eastern North Atlantic
579 (ACE-ENA), *Bulletin of the American Meteorological Society*, 103, E619-E641, 2022.
580 Wood: Stratocumulus Clouds, *Monthly Weather Review*, 140, 2373-2423, 10.1175/mwr-d-11-
581 00121.1, 2012.
582 Yang, F., Kollias, P., Shaw, R. A., and Vogelmann, A. M.: Cloud droplet size distribution
583 broadening during diffusional growth: ripening amplified by deactivation and reactivation,
584 *Atmospheric Chemistry and Physics*, 18, 7313-7328, 2018.
585 Yeom, J. M., Helman, I., Prabhakaran, P., Anderson, J. C., Yang, F., Shaw, R. A., and Cantrell,
586 W.: Cloud microphysical response to entrainment and mixing is locally inhomogeneous and
587 globally homogeneous: Evidence from the lab, *Proceedings of the National Academy of*
588 *Sciences*, 120, e2307354120, 2023.
589 Yeom, J. M., Yum, S. S., Shaw, R. A., La, I., Wang, J., Lu, C., Liu, Y., Mei, F., Schmid, B., and
590 Matthews, A.: Vertical variations of cloud microphysical relationships in marine stratocumulus
591 clouds observed during the ACE-ENA campaign, *Journal of Geophysical Research:*
592 *Atmospheres*, 126, e2021JD034700, 2021.
593 Yum, S. S., Wang, J., Liu, Y., Senum, G., Springston, S., McGraw, R., and Yeom, J. M.: Cloud
594 microphysical relationships and their implication on entrainment and mixing mechanism for the
595 stratocumulus clouds measured during the VOCALS project, *Journal of Geophysical Research:*
596 *Atmospheres*, 120, 5047-5069, 2015.

597

598

599



600

601 Figure 1: Illustration of experiment set up: a) the left panel illustrates aircraft measurements near
 602 cloud top. During 2s, the aircraft traverse 200 m, acquiring 10 samples. Each sample corresponds
 603 to a 20-m cloud parcel, which is simulated by the EMPM. The sampled cloud parcels exhibit
 604 varying entrainment fractions as indicated by the shading. Lighter (sparser) shading corresponds
 605 to samples with higher entrainment fractions. The right panel illustrates the simulated parcel
 606 experiencing three stages: ① rising, ② entrainment and ③ sinking. b) Illustration of the local and
 607 bulk-based perspective for simulations analysis: the local perspective tracks the change of
 608 properties with time after the entrainment events; the bulk perspective collects multiple parcels
 609 with various EF at a given time. t_1 represents the entrainment moment, t_n represents an arbitrary
 610 time step after entrainment.

611

612



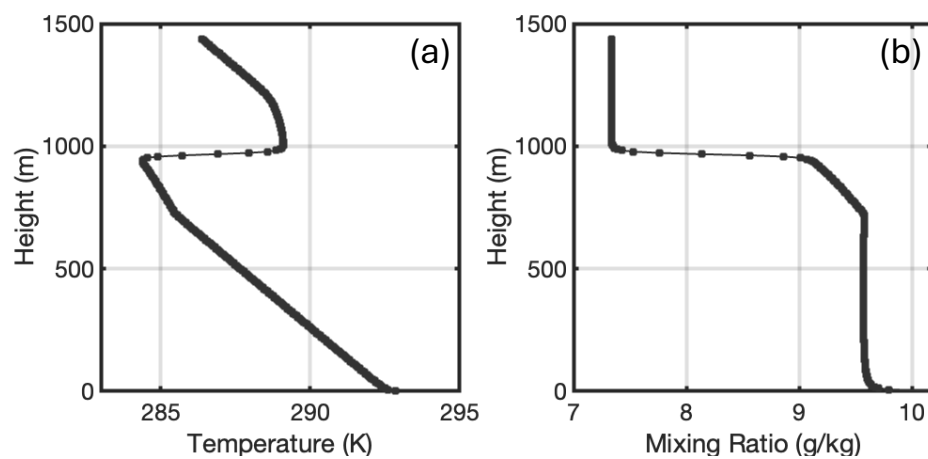
613

614

615

616

617



618

619 Figure 2: The idealized a) temperature and b) mixing ratio profiles based on the sounding
620 observation at 5:30 UTC on June 30th, 2017 during the ACE-ENA field campaign.

621



622

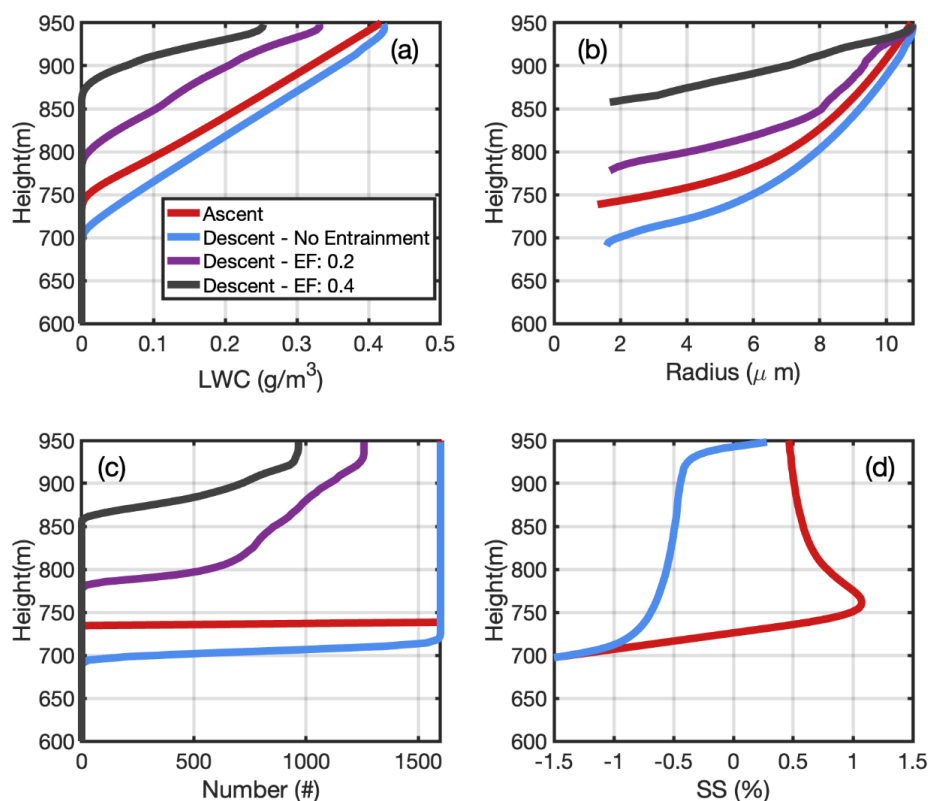
Table 1 – Model Configuration

Parameter	Control	Dry	Turbulent
Domain Length (m)		20m	
CCN Concentration (cm ⁻³)		80	
Vertical Air Velocity (ms ⁻¹)		±1	
Cloud Top Height (m)		950	
Aerosol Size Distribution		Monodisperse	
Initial mass of droplet solute (kg)		0.1122*10 ⁻¹⁷	
Initial aerosol radius (m)		0.216*10 ⁻⁶	
Type of aerosol		NaCl	
Eddy Dissipation Rate (m ² s ⁻³)	0.0025		0.01
Entrained air temperature (K)	285.77	288	285.77
Entrained air water vapor(g/kg)	8.6*10 ⁻³	7.9*10 ⁻³	8.6*10 ⁻³

623 Table 1: Model configurations for the control, dry and turbulent simulation experiment.



624



625

626 Figure 3: For the control experiment, domain-averaged cloud properties as function of height: a)
 627 LWC, b) radius, c) droplet number d) supersaturation. The red line represents the ascending parcel,
 628 while the blue, purple and black lines represent the descending parcel with entrainment fraction of
 629 0, 0.2 and 0.4 respectively. In (d) only the ascending parcel and the descending parcel with EF of
 630 0.4 is shown.

631

632

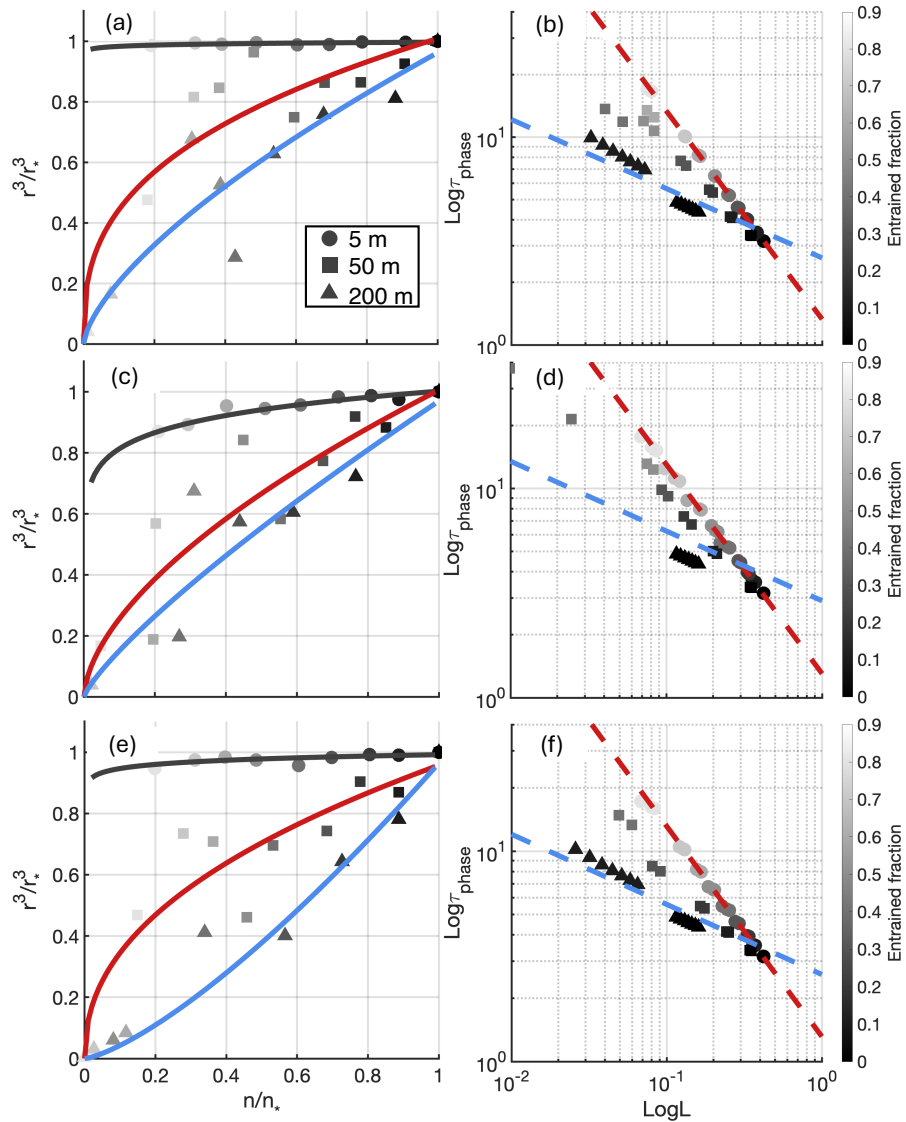
633

634

635

636

637



638

639 Figure 4: Mixing diagrams for three experiments: The left panel represents the $n-r^3$ mixing
 640 diagram for the (a) control, (c) dry and (e) turbulent experiment. The circle, square and triangle
 641 represents simulations at 5, 50 and 200m from cloud top. The black, red and blue lines represent
 642 the polynomial fitting of the parcels at each height level. The right panel indicates the $L-\tau_{\text{phase}}$
 643 mixing diagram for the (b) control, (d) dry and (f) turbulent experiment. The circle, square and
 644 triangle represents simulations at three heights as indicated in (a). The red, blue dashed line
 645 represents the IM and HM reference line with slope of -1 and -1/3.

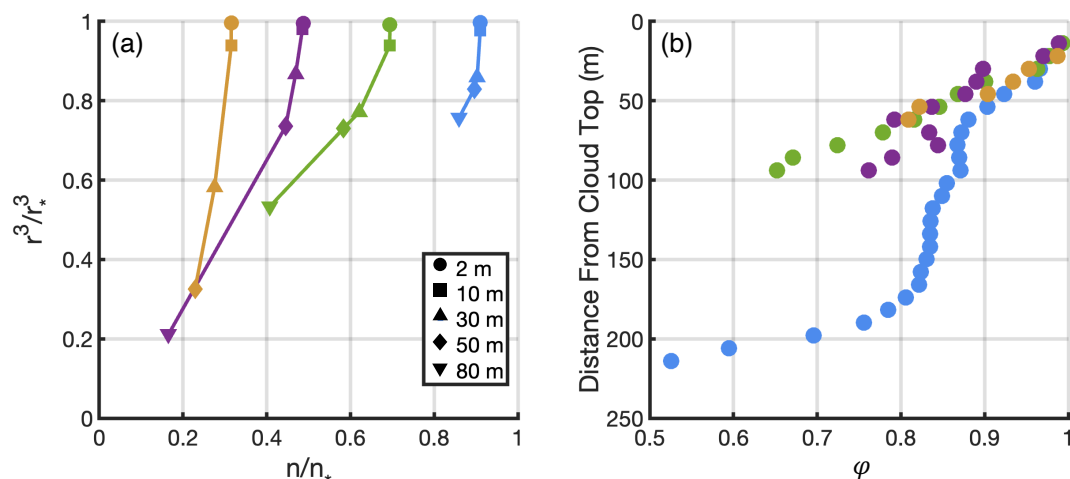
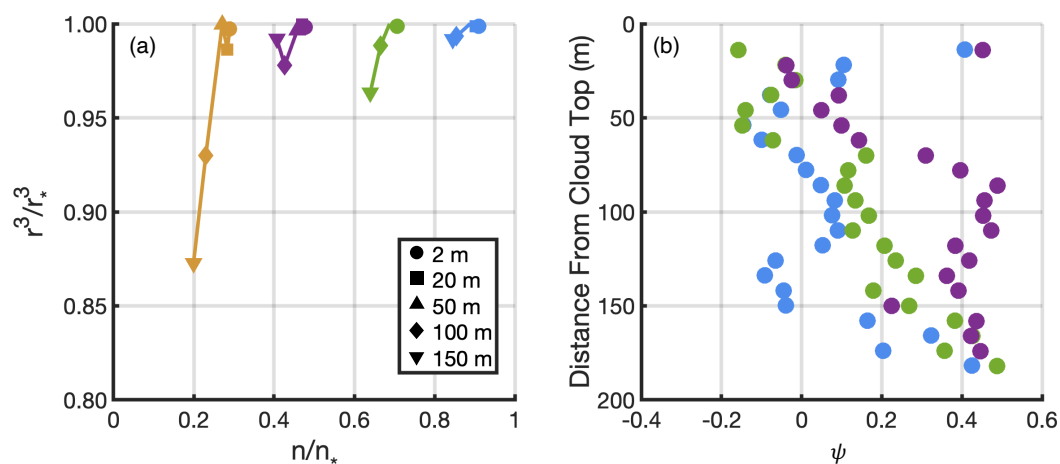


Figure 5: a) $n-r^3$ mixing diagram from the parcel-based perspective for the control experiment. The circle, square, triangle, diamond and the reverse-triangle indicate the height of 2m, 10m, 30m, 50m and 80m from cloud top. The blue, green, purple and yellow represents the parcel with EF of 0.1, 0.3, 0.5 and 0.7. b) The homogeneous mixing degree (ϕ) as a function of distance from cloud top, different color represents parcel with different EF as indicated in (a).



665



666

667 Figure 6: a) $n-r^3$ mixing diagram from the parcel-based perspective for the strict IM experiment.
 668 The circle, square, triangle, diamond and the reverse-triangle indicate the parcel at height of 2m,
 669 20m, 50m, 100m and 150m from cloud top. The blue, green, purple and yellow represents parcel
 670 with EF of 0.1, 0.3, 0.5 and 0.7. b) The homogeneous mixing degree (ψ) as a function height for
 671 the strict IM experiment. The blue, green, purple color represents parcel with EF of 0.1, 0.3, 0.5.

672

673

674

675

676

677

678

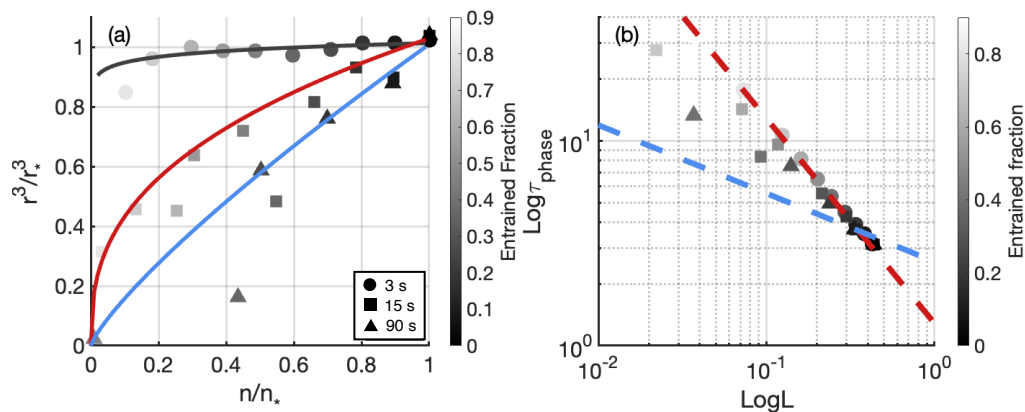
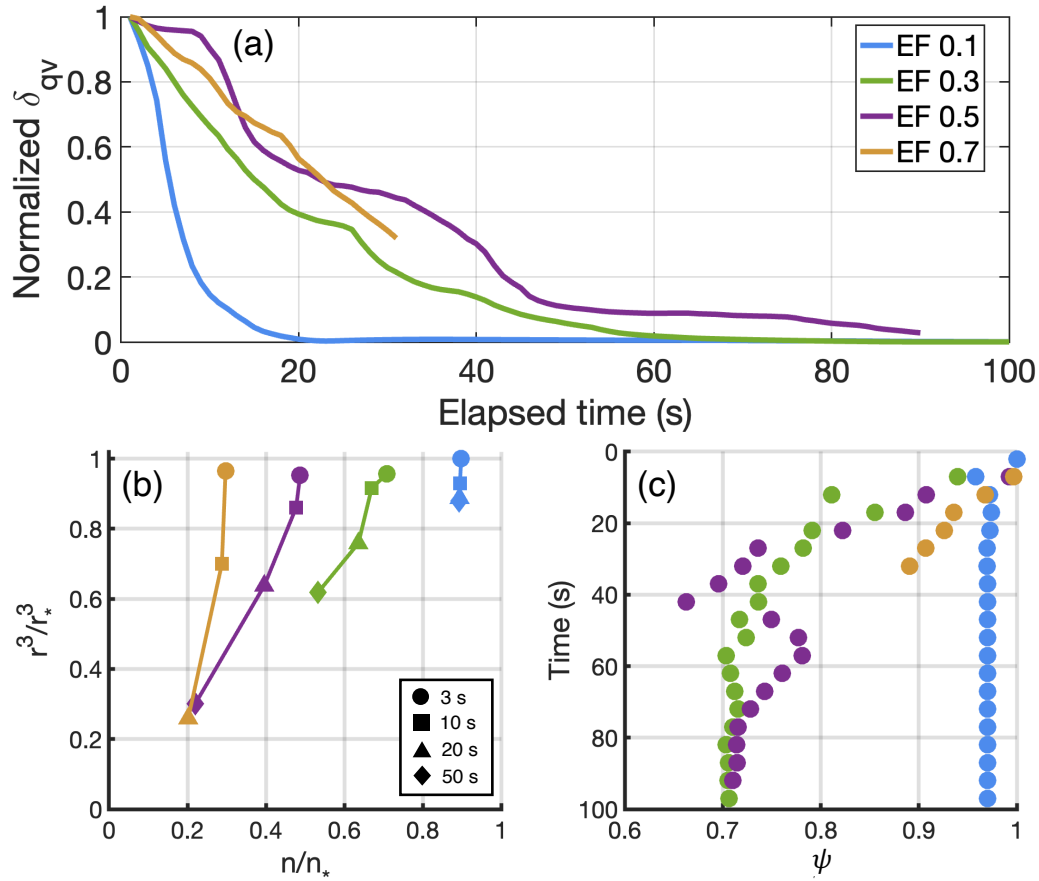


Figure 7: (a) $n-r^3$ mixing diagram from the bulk perspective for the isobaric mixing experiment: The circle, square and triangle represents the elapsed time of 3s, 15s and 90s after entrainment. The black, red and blue lines represent the polynomial fitting for the parcels at 3s, 15s and 90s, respectively. (b) $L-\tau_{\text{phase}}$ mixing diagram for the isobaric mixing experiment. The circle, square and triangle represents the elapsed time at 3s, 15s and 90s after entrainment. The red, blue dashed line represents the IM and HM reference line with slope of -1 and -1/3.



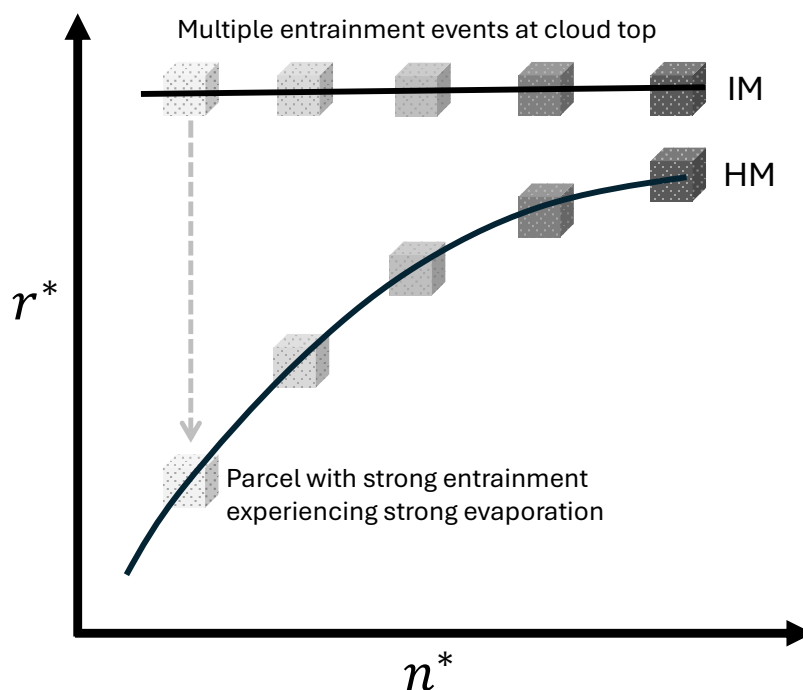
701



702

703 Figure 8: (a) Normalized standard deviation of water vapor (δ_{qv}) in the parcel after entrainment
 704 for the isobaric mixing experiment. The blue, green, purple and yellow line represents the parcel
 705 with EF of 0.1, 0.3, 0.5 and 0.7. (b) n - r^3 mixing diagram for the isobaric mixing experiment. The
 706 blue, green, purple and yellow symbol represents parcel with EF of 0.1, 0.3, 0.5 and 0.7. The circle,
 707 square, triangle and diamond indicate the parcel at elapsed time of 3s, 10s, 20s, 50s after
 708 entrainment. (c) The homogeneous mixing degree (ψ) as a function elapsed time for the isobaric
 709 mixing experiment. Different color represents parcel with different EF indicated in (b).

710



712

713 Figure 9: Illustration of the IM-HM transition within Sc from the bulk perspective. Parcels with
 714 darker (lighter) shading corresponds to samples with lower (higher) entrainment fractions. The
 715 horizontal black line represents the IM behavior occurring near cloud top, the curved line
 716 represents the HM behavior occurring within cloud.

717

718

719

720

721

722

723

724

725

726